

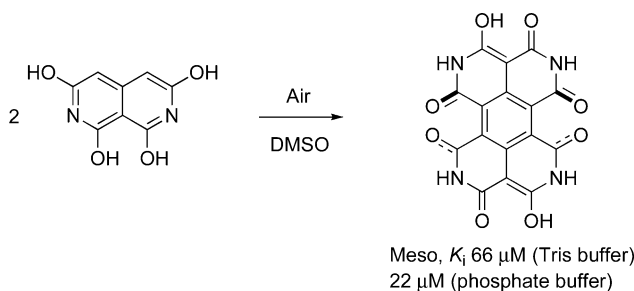
## A Novel Lumazine Synthase Inhibitor Derived from Oxidation of 1,3,6,8-Tetrahydroxy-2,7-naphthyridine to a Tetraazaperylenehexaone Derivative

Yanlei Zhang,<sup>†</sup> Boris Illarionov,<sup>‡</sup> Adelbert Bacher,<sup>‡</sup> Markus Fischer,<sup>‡</sup> Gunda I. Georg,<sup>§</sup> Qi-Zhuang Ye,<sup>§</sup> David Vander Velde,<sup>§</sup> Phillip E. Fanwick,<sup>#</sup> Yunlong Song,<sup>†</sup> and Mark Cushman<sup>\*,†</sup>

Department of Medicinal Chemistry and Molecular Pharmacology, School of Pharmacy and Pharmaceutical Sciences, and The Purdue Cancer Center, Purdue University, West Lafayette, Indiana 47907, Lehrstuhl für Organische Chemie und Biochemie, Technische Universität München, Lichtenbergstrasse 4, D-85747 Garching, Germany, Department of Medicinal Chemistry, University of Kansas, Lawrence, Kansas 66047, and Department of Chemistry, Purdue University, West Lafayette, Indiana 47907

cushman@pharmacy.purdue.edu

Received October 30, 2006



Air oxidation of 1,3,6,8-tetrahydroxy-2,7-naphthyridine afforded 2,5,8,11-tetraaza-5,11-dihydro-4,10-dihydroxyperylene-1,3,6,7,9,12-hexaone. X-ray crystallography of the product revealed that it exists in the meso form in the solid state. The mechanism of product formation most likely involves oxidative phenolic coupling and oxidation. The product proved to be a competitive inhibitor of *Schizosaccharomyces pombe* lumazine synthase with a  $K_i$  of  $66 \pm 13 \mu\text{M}$  in Tris buffer and  $22 \pm 4 \mu\text{M}$  in phosphate buffer. This is significantly more potent than the reactant ( $K_i$   $350 \pm 76 \mu\text{M}$ , competitive inhibition), which had previously been identified as a lumazine synthase inhibitor by high-throughput screening. Ab initio calculations indicate that the meso form is slightly less stable than the enantiomeric form, and that the two forms interconvert rapidly at room temperature.

### Introduction

Riboflavin (**4**, vitamin B<sub>2</sub>) is essential for life. It plays a crucial role in many biological processes, including photosynthesis and mitochondrial electron transport. Whereas animals obtain riboflavin from dietary sources, certain microorganisms such as Gram-negative pathogenic bacteria and yeasts lack an efficient riboflavin uptake system and are therefore absolutely dependent on endogenous riboflavin biosynthesis.<sup>1–4</sup> Riboflavin

biosynthesis is therefore an attractive target for the design and synthesis of new antibiotics, which are urgently needed because pathogens are becoming drug resistant at an alarming rate.

Lumazine synthase catalyzes the penultimate step in the biosynthesis of riboflavin (Scheme 1). Although the precise details remain to be established, the lumazine synthase-catalyzed reaction most likely proceeds along the mechanistic pathway involving Schiff base formation, phosphate elimination, tautomerization, ring closure, and dehydration.<sup>5</sup>

High-throughput screening (HTS) employs large libraries of compounds to identify those of biological interest. We recently

\* Corresponding author. E-mail: cushman@pharmacy.purdue.edu.  
<sup>†</sup> Department of Medicinal Chemistry and Molecular Pharmacology, Purdue University.

<sup>‡</sup> Technische Universität München.

<sup>§</sup> University of Kansas.

<sup>#</sup> Department of Chemistry, Purdue University.

(1) Wang, A. *I Chuan Hsueh Pao* **1992**, *19*, 362–368.

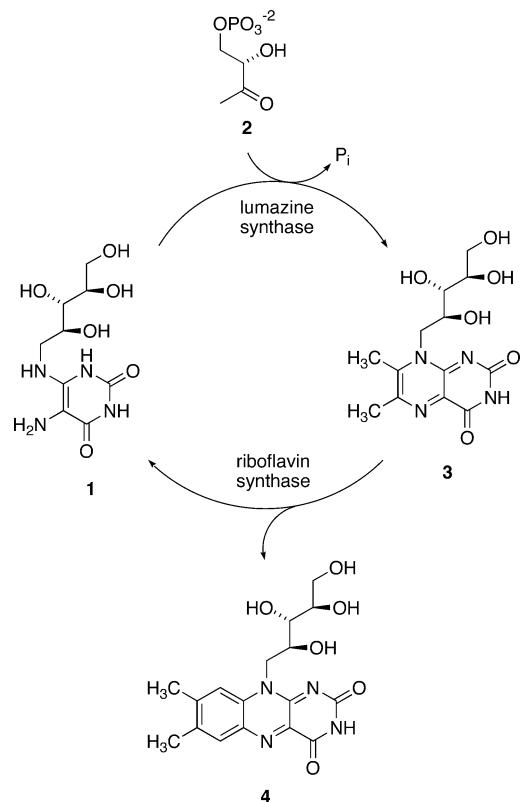
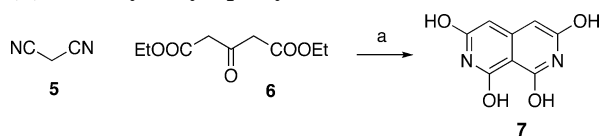
(2) Oltmanns, O.; Lingens, F. *Z. Naturforschung* **1967**, *22 b*, 751–754.

(3) Logvinenko, E. M.; Shavlovsky, G. M. *Mikrobiologiya* **1967**, *41*, 978–979.

(4) Neuberger, G.; Bacher, A. *Biochem. Biophys. Res. Commun.* **1985**, *127*, 175–181.

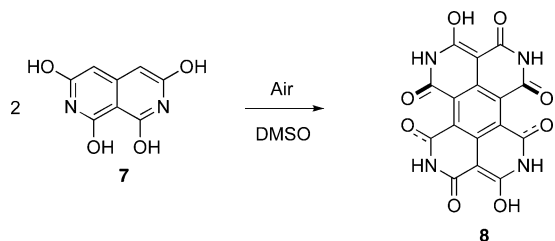
(5) Volk, R.; Bacher, A. *J. Am. Chem. Soc.* **1988**, *110*, 3651–3653.

## SCHEME 1. Biosynthesis of Riboflavin

SCHEME 2. Synthesis of 1,3,6,8-Tetrahydroxynaphthyridine (7)<sup>a</sup>

<sup>a</sup> Reagents and conditions: (a) (1) EtOH, Et<sub>2</sub>NH, 23 °C (48 h); (2) H<sub>2</sub>SO<sub>4</sub>, heat (10 min), then dilute with H<sub>2</sub>O.

## SCHEME 3. Formation of Tetraazaperylenehexaone System 8



developed a high-throughput screen utilizing the fluorescence of riboflavin for identification of lumazine synthase inhibitors.<sup>6</sup> The method utilizes the displacement of riboflavin, which is fluorescent, from a nonfluorescent complex of *Schizosaccharomyces pombe* lumazine synthase with riboflavin. High-throughput screening of a commercial library of about 100 000 compounds using this assay resulted in the identification of a 1,3,6,8-tetrahydroxynaphthyridine (7)<sup>7</sup> as a potential lumazine synthase inhibitor. The present communication describes the

(6) Chen, J.; Illarionoc, B.; Bacher, A.; Fischer, M.; Haase, I.; Georg, G.; Ye, Q.-z.; Ma, Z.; Cushman, M. *Anal. Biochem.* **2005**, *338*, 124–130.

(7) Ferrier, B. M.; Campbell, N. *J. Chem. Soc.* **1960**, 3513–3515.

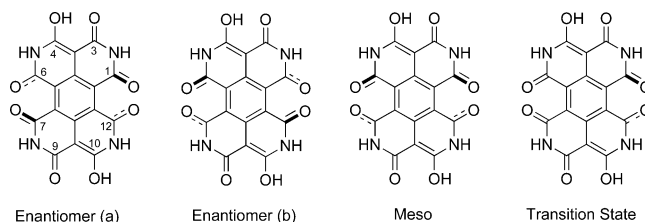


**FIGURE 1.** Stereoisomers of the tetraazaperylenehexaone system **8**. The transition state depicted is the one between enantiomer (a) and the meso compound.

characterization and confirmation of **7** as a lumazine synthase inhibitor as well as its conversion to a more active compound.

## Results and Discussion

In order to confirm the structure of naphthyridine **7**, samples of it were obtained both commercially (Aldrich Chemical Co.) and also by synthesis from malononitrile (**5**) and diethyl acetonedicarboxylate (**6**) in refluxing ethanol containing a catalytic amount of diethylamine (Scheme 2). Removal of the solvent yielded a residue that was treated with sulfuric acid and then diluted with water to provide the desired product **7** (mp >350 °C, EIHRMS *m/z* calcd for C<sub>8</sub>H<sub>6</sub>N<sub>2</sub>O<sub>4</sub> 195.0406, found 195.0403). The <sup>1</sup>H NMR and <sup>13</sup>C NMR spectra of **7** indicate that it exists in solution as a complex mixture of amide and lactim tautomers. Enzyme kinetics revealed that the synthetic naphthyridine **7** prepared in our laboratories is a relatively weak *S. pombe* lumazine synthase inhibitor with a *K*<sub>i</sub> of 350 ± 76 μM. This was less potent than the commercial sample of **7**, and more detailed studies revealed that the potency of the synthetic sample seemed to increase on storage in solution. In view of these results, an effort was made to characterize the synthetic material in more detail and to investigate the possible reasons for the observed increase in potency on storage of the synthetic material in solution.

During the characterization of naphthyridine **7**, a sample of it was dissolved in DMSO and the solution was left standing open to air for a week. This resulted in a change in color of the solution from yellow to dark red. After a month, dark red needles crystallized from the solution. X-ray crystallography revealed that the red needles were 2,5,8,11-tetraaza-5,11-dihydro-4,10-dihydroxyperylene-1,3,6,7,9,12-hexaone (**8**, Scheme 3).

Because of steric hindrance between the two carboxyl oxygens at C-6 and C-7, as well as at C-1 and C-12, the perylenehexaone system **8** can theoretically exist in a number of stereoisomeric forms. If one only considers the three stereoisomers in which these pairs of carbonyl oxygens are on opposite sides of the ring system, the tetraazaperylenehexaone **8** can exist either as a meso compound or as a pair of two enantiomers (Figure 1). The crystal structure space group was determined to be *P1* (No. 2), which is only consistent with the tetraazaperylenehexaone **8** existing in the solid state as the meso compound. The crystal structure of **8**, which contains two solvent-derived molecules of DMSO, is displayed in Figure 2. The orientations of the carbonyl oxygens at C-6, C-7, C-1, and C-12 are clearly visible from the crystal structure, which also proves that the tetraazaperylenehexaone **8** crystallized in the meso form and not as the racemate.

The mechanism of the reaction leading to the tetraazaperylenehexaone **8** most likely involves oxidative phenolic coupling of the radical species **9** and **10**, followed by a four-electron oxidation (Scheme 4). Oxidative C–C coupling reactions of phenols are well-known processes that are usually catalyzed by

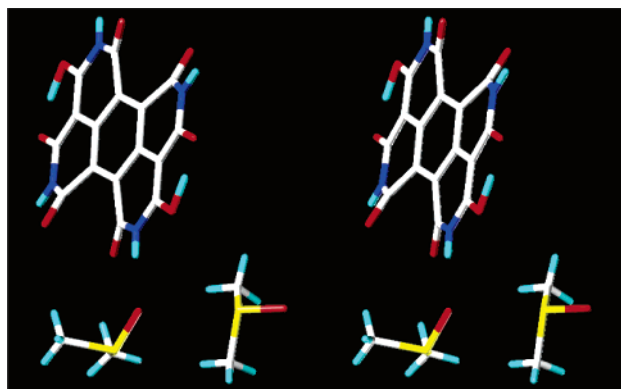
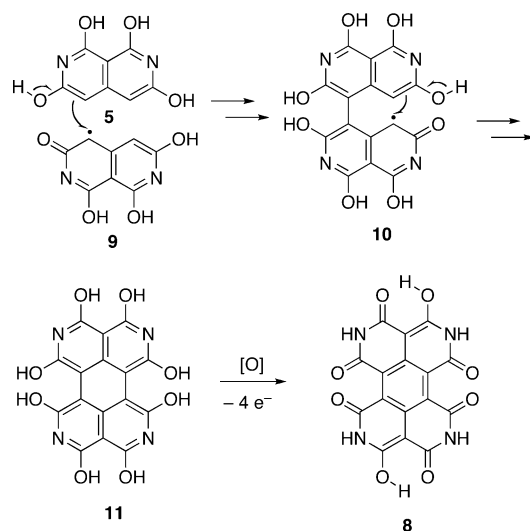


FIGURE 2. Stereoview of the crystal structure of **8**. The diagram is programmed for wall-eyed (relaxed) viewing.

**SCHEME 4. Oxidative Phenolic Coupling and Oxidation Pathway Leading to the Tetraazaperylenehexaone System **8****



metals (typically copper),<sup>8–10</sup> dicopper–dioxygen complexes,<sup>11</sup> enzymes,<sup>10,12,13</sup> or various reactive oxygen species.<sup>14</sup> In the present case the oxidant is unidentified. The reaction mixture was left open to the atmosphere for a period of a month before the product began to crystallize from solution.

Surprisingly, the tetraazaperylenehexaone system **8** proved to be a more potent inhibitor of *S. pombe* lumazine synthase than the original HTS hit compound **7**. As mentioned above, the  $K_i$  of the original compound **7** was of  $350 \pm 76 \mu\text{M}$ , while that of the oxidative phenolic coupling product **8** was  $66 \pm 13 \mu\text{M}$  in Tris buffer, pH 7.0.

Molecular modeling was performed in order to investigate the binding of the meso isomer of compound **8** to the enzyme.

(8) Sun, H. J.; Harms, K.; Sundermeyer, J. *J. Am. Chem. Soc.* **2004**, *126*, 9550–9551.

(9) Li, X. L.; Hewgley, J. B.; Mulrooney, C. A.; Yang, J. M.; Kozlowski, M. C. *J. Org. Chem.* **2003**, *68*, 5500–5511.

(10) Orlandi, M.; Rindone, B.; Molteni, G.; Rummakko, P.; Brunow, G. *Tetrahedron* **2001**, *57*, 371–378.

(11) Osako, T.; Ohkubo, K.; Taki, M.; Tachi, Y.; Fukuzumi, S.; Itoh, S. *J. Am. Chem. Soc.* **2003**, *125*, 11027–11033.

(12) Nezbedová, L.; Hesse, M.; Drandarov, K.; Bigler, L.; Werner, C. *Planta* **2001**, *213*, 411–417.

(13) Ward, G.; Hadar, Y.; Bilkis, I.; Dosoretz, C. G. *J. Biol. Chem.* **2003**, *278*, 39726–39734.

(14) Shamovsky, I. L.; Riopelle, R. J.; Ross, G. M. *J. Phys. Chem. A* **2001**, *105*, 1061–1070.

TABLE 1. Inhibition Constants vs *S. pombe* Lumazine Synthase

compd	mechanism	$K_s$ ( $\mu\text{M}$ )	$k_{\text{cat}}$ , $\text{min}^{-1}$	$K_i$ ( $\mu\text{M}$ )
<b>7</b>	competitive	$6.9 \pm 1.6^a$	$5.9 \pm 0.7^a$	$350 \pm 76^a$
<b>8</b>	competitive	$1.7 \pm 0.2^a$	$3.9 \pm 0.1^a$	$66 \pm 13^a$
<b>8</b>	competitive	$0.44 \pm 0.07^b$	$5.3 \pm 0.1^b$	$22 \pm 4^b$

<sup>a</sup> Assay buffer: 50 mM Tris-HCl, pH 7.0, 100 mM NaCl, 5 mM EDTA, 5 mM DTT, reaction mixture volume 1 mL. 5-Amino-6-ribitylamino-pyrimidinedione concentration range, 2 – 20  $\mu\text{M}$ ; 3,4-dihydroxy-2-butanone-4-phosphate, 100  $\mu\text{M}$ ; compound concentrations 0, 20, 40, 80  $\mu\text{M}$ . <sup>b</sup> Assay buffer: 100 mM K/Na-phosphate, pH 7.0, 5 mM EDTA, 5 mM DTT, reaction mixture volume 1 mL. 5-Amino-6-ribitylamino-pyrimidinedione concentration range, 1.5 – 15  $\mu\text{M}$ ; 3,4-dihydroxy-2-butanone-4-phosphate, 100  $\mu\text{M}$ ; compound concentrations 0, 25, 50, 75  $\mu\text{M}$ .

Both inorganic phosphate and riboflavin were removed from the structure of the *S. pombe* lumazine synthase complex with riboflavin (PDB code 1KYV),<sup>15</sup> and the oxidation product **8** was then docked into the apoenzyme structure using Gold software (BST, version 3.0, 2005). The reason that the inorganic phosphate was removed from the structure before docking **8** was that the inhibition assay was initially carried out in phosphate-free buffer. Energy minimization was then performed using Sybyl 7.1. The resulting structure is displayed in Figure 3. According to the theoretical model, the binding of the red dimer **8** in the active site of *S. pombe* lumazine synthase is similar to that of riboflavin (**4**), as well as to that of substrate and product analogues.<sup>15</sup> As with riboflavin (**4**) and the substrate and product analogues **12**<sup>16,17</sup> and **13**,<sup>17–19</sup> the binding is stabilized by stacking interactions involving Tyr27 and His94 (Figure 3).<sup>15</sup> In addition, the binding of the red dimer **8** to the enzyme could be mediated by hydrogen bonding interactions involving the backbone NH of Ile88, the backbone carbonyl of Val86, and the backbone NH of Ser62 (Figure 3). Similar protein contacts are evident at the pyrimidinedione rings in the crystal structures of riboflavin (**4**) and the substrate and product analogues **12** and **13**. However, additional contacts are possible with the red dimer **8** that are not present with the other ligands. These include hydrogen-bonding contacts with the side chain guanidine moiety of Arg133, the side chain hydroxyl of Thr92, and water-mediated contacts with Trp146 and Asp145. Taken together, the molecular modeling results indicate that the binding of the red dimer **8** in the active site of *S. pombe* lumazine synthase is certainly plausible; it is also reasonable that it could be stabilized by some of the same forces that stabilize the binding of riboflavin (**4**), the substrate analogue **12**, and the product analogue **13**. This point is emphasized in Figure 4, which shows how the red dimer **8** is calculated to bind compared to the observed position of riboflavin (**4**) in the crystal structures. It is clear from Figure 4 that there is considerable overlap in the space occupied by riboflavin and the space calculated to be occupied by the red dimer **8**.

The inhibition constants specified above were determined in Tris buffer at pH 7.0. Since in some cases the presence of inorganic phosphate has previously been demonstrated to affect the binding constants of lumazine synthase inhibitors, the

(15) Gerhardt, S.; Haase, I.; Steinbacher, S.; Kaiser, J. T.; Cushman, M.; Bacher, A.; Huber, R.; Fischer, M. *J. Mol. Biol.* **2002**, *318*, 1317–1329.

(16) Cresswell, R. M.; Wood, H. S. C. *J. Chem. Soc.* **1960**, 4768–4775.

(17) Al-Hassan, S. S.; Kulick, R. J.; Livingston, D. B.; Suckling, C. J.; Wood, H. C. S.; Wrigglesworth, R.; Ferone, R. *J. Chem. Soc., Perkin Trans. I* **1980**, 2645–2656.

(18) Suzuki, A.; Goto, M. *Bull. Chem. Soc. Jpn.* **1971**, *44*, 1869–1872.

(19) Cushman, M.; Yang, D.; Gerhardt, S.; Huber, R.; Fischer, M.; Kis, K.; Bacher, A. *J. Org. Chem.* **2002**, *67*, 5807–5816.

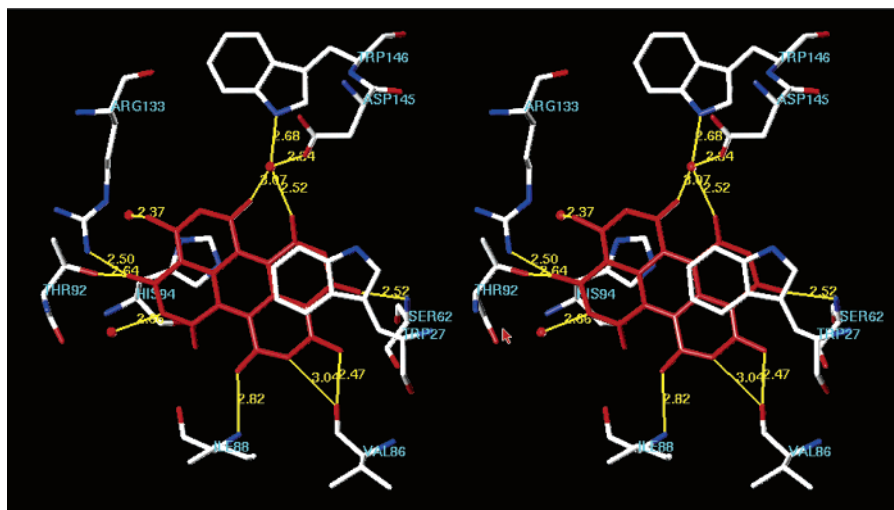


**FIGURE 3.** Hypothetical structure of the meso conformer of the red dimer **8** bound in the active site of *S. pombe* lumazine synthase without inorganic phosphate. The dimer is red, and the amino acid residues are colored by atom type. The diagram is programmed for wall-eyed (relaxed) viewing.

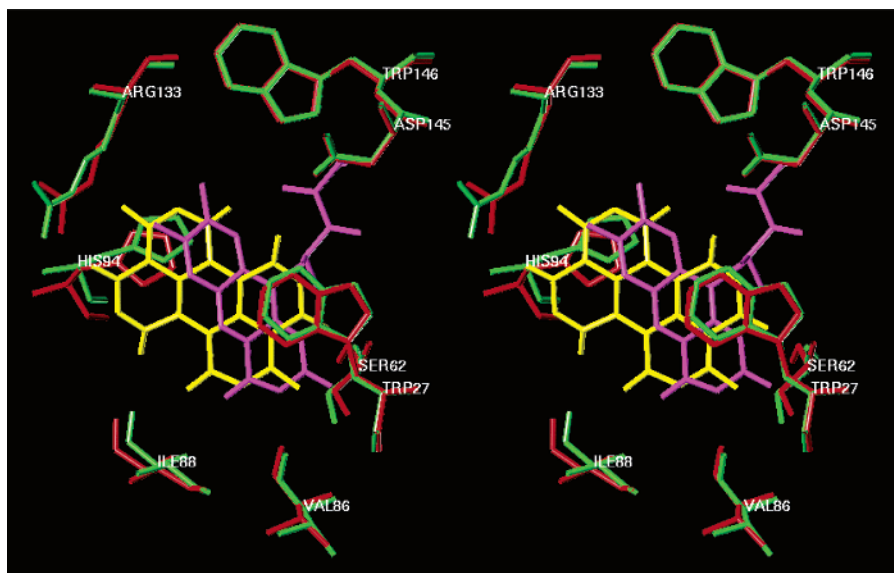
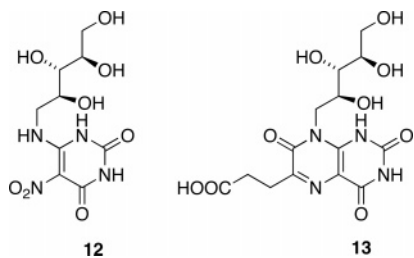


**FIGURE 4.** Hypothetical structure of the meso conformer of the red dimer **8** bound in the active site of *S. pombe* lumazine synthase superimposed on the crystal structure of riboflavin (**4**) bound in the active site of *S. pombe* lumazine synthase. Yellow: dimer **8**, magenta: riboflavin (**4**); red, theoretical locations of amino acid residues in the enzyme/**8** complex; green: amino acid residues in the crystal structure of the enzyme/**4** complex. The diagram is programmed for wall-eyed (relaxed) viewing.



binding of the red dimer **8** was also studied in phosphate buffer at pH 7.0. The results of the inhibition experiments vs *S. pombe* lumazine synthase are listed in Table 1. The results reveal that the red dimer **8** is a more potent inhibitor of *S. pombe* lumazine synthase in the presence of phosphate, producing a  $K_i$  of 22  $\mu\text{M}$  in phosphate buffer as opposed to 66  $\mu\text{M}$  in Tris buffer. Competitive inhibition occurred in each case as indicated by

analysis of the Lineweaver–Burke enzyme kinetics plots using the DynaFit program<sup>20</sup> (Figure 5).

The crystal structure of *S. pombe* lumazine synthase complex with riboflavin (PDB code 1KYV)<sup>15</sup> contains an inorganic phosphate molecule that occupies the binding site of the organic phosphate moiety present in the substrate **2** (Scheme 2). The increase in inhibitory potency of the red dimer **8** in phosphate buffer is significant because inorganic phosphate could possibly be present in the active site of lumazine synthase under cellular conditions, although if present it would obviously have to be displaced by the phosphate of the substrate **2** during catalysis. In order to gain insight into the increased potency of **8** in the presence of phosphate, it was docked in the active site of the enzyme with phosphate bound using the Gold docking program, and the model resulting after energy minimization using the

(20) Kuzmic, P. *Anal. Biochem.* **1996**, *237*, 260–273.

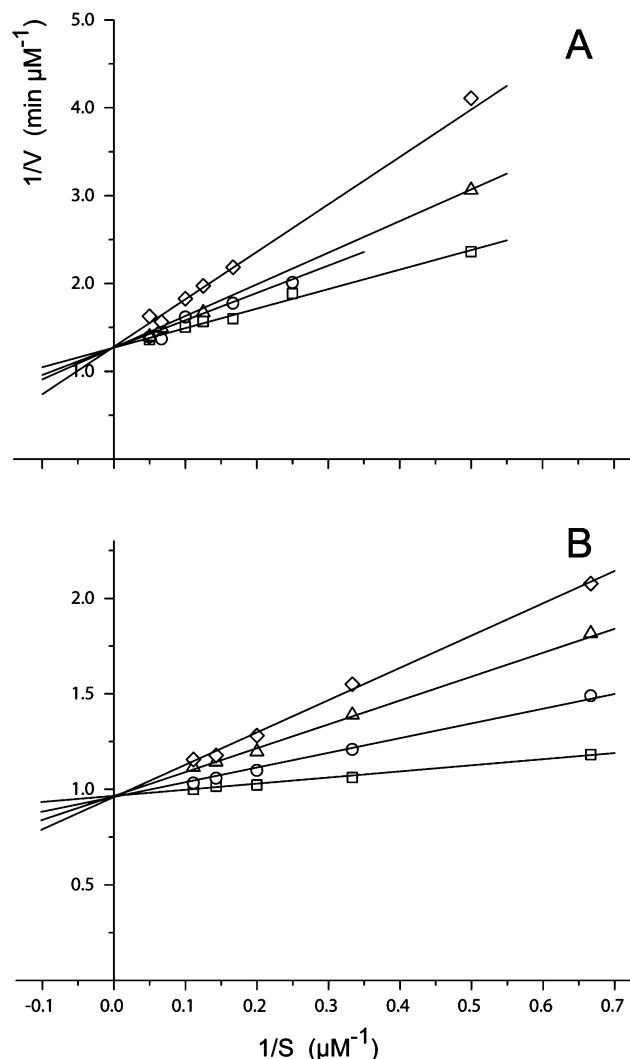


**FIGURE 5.** Lineweaver–Burk plots for the inhibition of *S. pombe* lumazine synthase by inhibitor **8**. Panel A; reaction buffer: 50 mM Tris-HCl pH 7.0, 100 mM NaCl, 5 mM EDTA, 5 mM DTT; inhibitor concentrations: (□) 0  $\mu\text{M}$ , (○) 20  $\mu\text{M}$ , (△) 40  $\mu\text{M}$ , (◇) 80  $\mu\text{M}$ ; mechanism, competitive. Panel B; reaction buffer: 100 mM K/Na-phosphate pH 7.0, 5 mM EDTA, 5 mM DTT; inhibitor concentrations: (□) 0  $\mu\text{M}$ , (○) 25  $\mu\text{M}$ , (△) 50  $\mu\text{M}$ , (◇) 75  $\mu\text{M}$ ; mechanism, competitive. The kinetic data were fitted with a nonlinear regression method by the program DynaFit.<sup>20</sup>

MMFF94s force field within Sybyl 7.1 is displayed in Figure 6. The model indicates that the increased potency in the presence of phosphate could be due to hydrogen bonding of one of the imide moieties present in the red dimer **8** to the inorganic phosphate molecule in the active site of the enzyme.

In addition to the meso conformer of the red dimer **8**, the two enantiomeric conformers (**a** and **b**) (Figure 1) were docked in the active site of the enzyme in the absence of phosphate (Figure 7) and the energies of the complexes minimized. Interestingly, the molecular mechanics energy calculations (Table 2) argue that the complex derived from the meso conformer is more stable than those derived from either of the enantiomers, and that the binding energy of the meso form to the enzyme is more favorable than either enantiomer. Furthermore, while the planes of all three ligand structures overlapped closely, and the orientations of the meso form and enantiomer **a** were very close, enantiomer **b** was rotated approximately 90°

relative to the other two (Figure 7). The calculated protein structures of all three complexes overlapped very closely, even though the protein structure was allowed to move during energy minimization. The three structures used to construct Figure 7 are displayed individually in the Supporting Information, together with the hydrogen-bonding contacts between the ligands and the protein structure.

Ab initio quantum mechanics calculations were performed with Gaussian 03 in order to estimate the relative energies of the meso and enantiomeric forms, as well as the transition state between the two forms. Among the ab initio techniques, density functional theory has been well established as a powerful tool that, in contrast to HF theory, includes electron correlation. However, there are reports that DFT may in some cases underestimate transition state barriers.<sup>21</sup> Therefore, the results of both DFT and HF calculations were obtained and both are listed in Table 3.

Starting from the crystal structure of the meso isomer of compound **8**, the structures of both enantiomers were built and fully optimized using the MOPAC AM1 method (with molecular mechanics correction of the CONH bonds, implemented within Sybyl 7.1). The three forms were then optimized using the restricted Hartree–Fock equation and the 3-21G basis set. The QST3 method was used to locate the transition state for the conversion of the meso form to one of the enantiomers using RHF/3-21G within Gaussian 03 (Revision C.02).<sup>22</sup> The meso form and the two enantiomers were further optimized using RHF/6-31G(d) and finally refined using density functional theory at B3LYP/6-31G(d). The results of these calculations are summarized in Table 3. The meso form and one of the enantiomers obtained from RHF/6-31G(d) optimization, and the transition state obtained from the RHF/3-21G QST3 calculations, were used in a QST3 calculation to locate the transition state at RHF/6-31G(d). Similarly, the meso form and one of the enantiomers obtained from B3LYP/6-31G(d) optimization, and the transition state obtained from the RHF/6-31G(d) QST3 calculations were used in a QST3 calculation to locate the transition state at B3LYP/6-31G(d), which represents the final transition state structure used in this study. The optimized structures of the meso form, one of the two enantiomers, and the calculated transition state are displayed in Figure 8. Frequency check calculation on the transition state structure obtained from DFT calculations yielded only one negative (imaginary) frequency ( $-105.3\text{ cm}^{-1}$ ), indicating a valid transition state. The vibrational mode of the imaginary frequency displayed in Figure 9 corresponds precisely to the transition

(21) Bach, R. D.; Glukhovtsev, M. N.; Gonzalez, C.; Marquez, M.; Estévez, C. M.; Baboul, A. G.; Schlegel, H. B. *J. Phys. Chem. A* **1997**, *101*, 6092–6100.

(22) Frisch, M. J.; Trucks, G. W.; Schlegel, H. B.; Scuseria, G. E.; Robb, M. A.; Cheeseman, J. R.; Montgomery, J. J. A.; Vreven, T.; Kudin, K. N.; Burant, J. C.; Millam, J. M.; Iyengar, S. S.; Tomasi, J.; Barone, V.; Mennucci, B.; Cossi, M.; Scalmani, G.; Rega, N.; Petersson, G. A.; Nakatsuji, H.; Hada, M.; Ehara, M.; Toyota, K.; Fukuda, R.; Hasegawa, J.; Ishida, M.; Nakajima, T.; Honda, Y.; Kitao, O.; Nakai, H.; Klene, M.; Li, X.; Knox, J. E.; Hratchian, H. P.; Cross, J. B.; Adamo, C.; Jaramillo, J.; Gomperts, R.; Stratmann, R. E.; Yazyev, O.; Austin, A. J.; Cammi, R.; Pomelli, C.; Ochterski, J. W.; Ayala, P. Y.; Morokuma, K.; Voth, G. A.; Salvador, P.; Dannenberg, J. J.; Zakrzewski, V. G.; Dapprich, S.; Daniels, A. D.; Strain, M. C.; Farkas, O.; Malick, D. K.; Rabuck, A. D.; Raghavachari, K.; Foresman, J. B.; Ortiz, J. V.; Cui, Q.; Baboul, A. G.; Clifford, S.; Cioslowski, J.; Stefanov, B. B.; Liu, G.; Liashenko, A.; Piskorz, P.; Komaromi, I.; Martin, R. L.; Fox, D. J.; Keith, T.; Al-Laham, M. A.; Peng, C. Y.; Nanayakkara, A.; Challacombe, M.; Gill, P. M. W.; Johnson, B.; Chen, W.; Wong, M. W.; Gonzalez, C.; Pople, J. A. Gaussian Revision B.05 ed. Pittsburgh, PA, 2003.

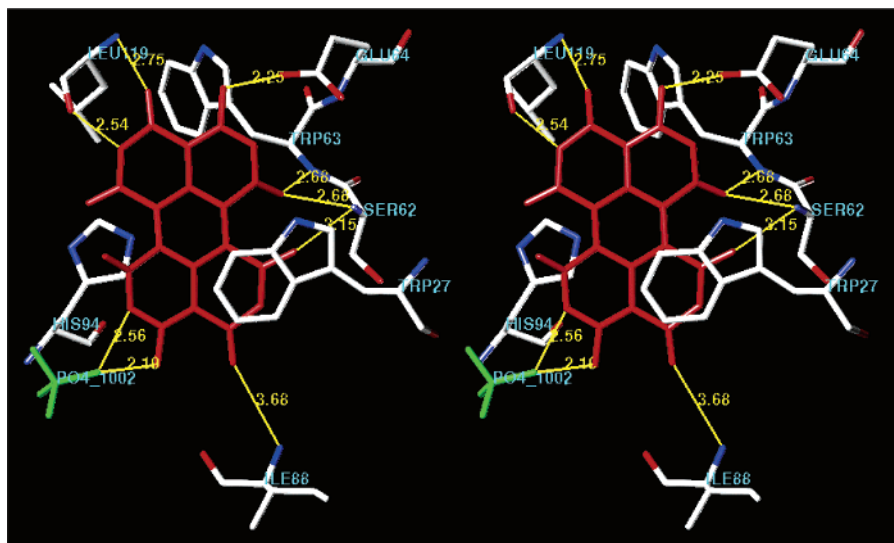


**FIGURE 6.** Hypothetical structure of the meso conformer of the red dimer **8** bound in the active site of *S. pombe* lumazine synthase with inorganic phosphate. The dimer is red, phosphate is green, and the amino acid residues are colored by atom type. The diagram is programmed for wall-eyed (relaxed) viewing.

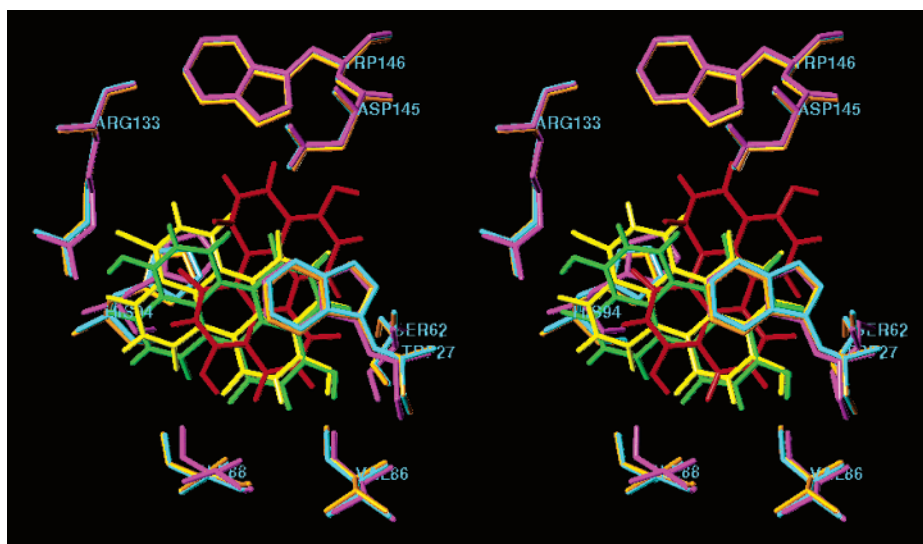


**FIGURE 7.** Overlay of the three hypothetical structures derived from docking and energy minimization of the complexes of the enzyme with the meso (yellow), enantiomer **a** (green), and enantiomer **b** (red) conformers of the red dimer **8**. The overlapping protein residues are those in the complexes derived from the meso (orange), enantiomer **a** (cyan), and enantiomer **b** (magenta) conformers.

**TABLE 2.** The Binding Energies of the Meso and Enantiomeric Structures of the Red Dimer **8**<sup>a</sup>

	$E_{\text{complex}}$	$E_{\text{enzyme}}$	$E_{\text{ligand}}$	$E_{\text{binding}}$	Gold Fitness
meso	-281.07	-162.79	14.58	-132.86	41.31
enantiomer <b>a</b>	-258.21	-162.79	13.81	-109.23	41.38
enantiomer <b>b</b>	-264.24	-162.79	13.81	-115.26	41.21

<sup>a</sup> All the energies were calculated using the MMFF94s force field and MMFF94 charges implemented in Sybyl 7.1 and are expressed in kcal/mol.  $E_{\text{enzyme}}$  indicates the energy of the minimized apoenzyme;  $E_{\text{complex}}$  indicates the energies of the final minimized complexes after ligand binding;  $E_{\text{ligand}}$  indicates the energies of the minimized ligand structures after extraction from the corresponding complex;  $E_{\text{binding}} = E_{\text{complex}} - E_{\text{ligand}} - E_{\text{enzyme}}$ ; Gold Fitness is the Gold fitness score.

state for conversion of the meso form to one of the enantiomers. The transition state structure has two of the carbonyls on one side in the same plane, and on the other side one carbonyl is “up” and one is “down”.

At all of the levels of theory, the activation energy differences are within 2.0 kcal/mol and in good agreement with each other (Table 3). The differences in the calculated values could reflect differences in the optimized geometries at various levels as well as differences in the levels of theory. The results of the DFT quantum mechanics calculations indicate that the meso form is 1.5 kcal/mol higher in energy than the enantiomeric form. The activation energy in going from the meso form to the transition state is 4.9 kcal/mol, and the activation energy in going from one of the enantiomers to the transition state is 6.4 kcal/mol (Figure 10). On the basis of these theoretical calculations, the meso and enantiomeric forms interconvert rapidly at room temperature. It can also be expected that the crystalline meso form is rapidly converted to the more stable racemate after dissolution. However, the enzyme-bound form is not certain, and the possibility exists that the meso and enantiomeric forms could interconvert while enzyme bound, or that the equilibrium

TABLE 3. The Calculated Energies of the Meso, Enantiomeric, and Transition State Structures of the Red Dimer 8

subject	RHF/3-21G	RHF/6-31G(d)	DFT/6-31G(d)
meso	-1418.27218350 Hartree <sup>a</sup>	-1426.24223124 Hartree	-1434.24688703 Hartree
enantiomer a	-1418.27470233 Hartree	-1426.24398674 Hartree	-1434.24927566 Hartree
transition state	-1418.26516725 Hartree	-1426.23251288 Hartree	-1434.23906710 Hartree
$\Delta E = E_{TS} - E_{meso}$	4.4 kcal/mol	6.1 kcal/mol	4.9 kcal/mol
$\Delta E = E_{meso} - E_{enantiomer}$	1.6 kcal/mol	1.1 kcal/mol	1.5 kcal/mol
$\Delta E = E_{TS} - E_{enantiomer}$	6.0 kcal/mol	7.2 kcal/mol	6.4 kcal/mol
TS negative frequency	-98.7 cm <sup>-1</sup>	-111.3 cm <sup>-1</sup>	-105.3 cm <sup>-1</sup>

<sup>a</sup> 1 Hartree (au) = 627.51 kcal/mol = 2625.500 kJ/mol.

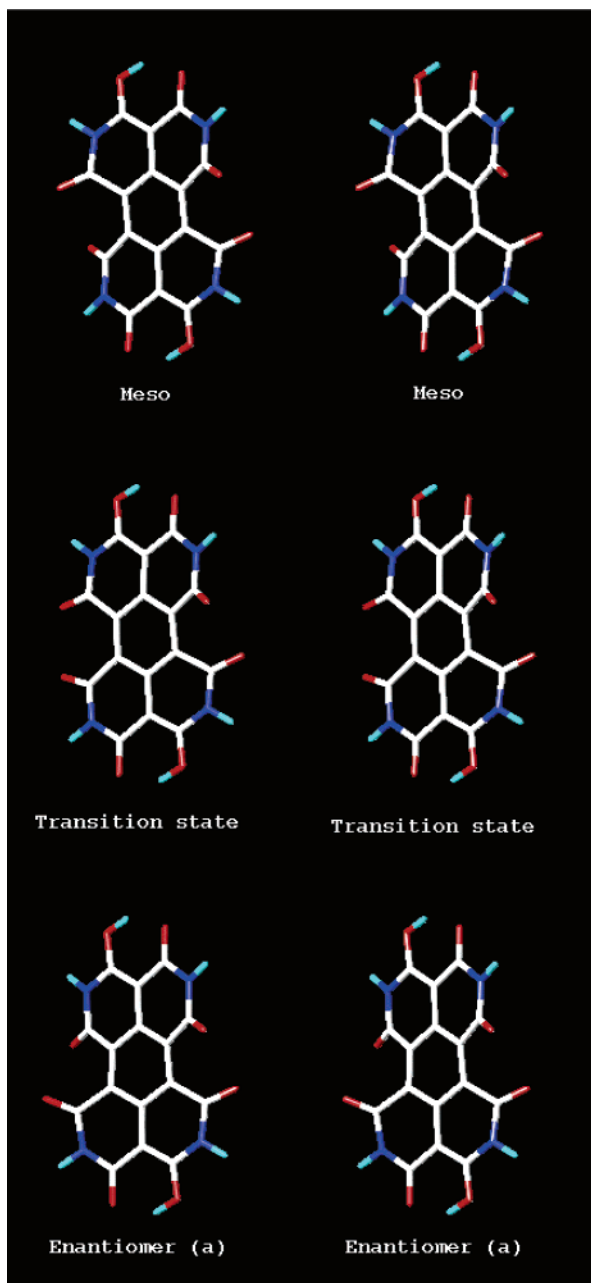


FIGURE 8. Stereoview of the meso form, enantiomer a, and corresponding transition state obtained from B3LYP/6-31G(d) calculations. The transition state structure corresponds to that depicted in Figure 1. The diagram is programmed for wall-eyed (relaxed) viewing.

could be shifted in the bound form to favor either the meso form or one of the enantiomeric forms. Although these calculations were performed in vacuo, the results should provide a valid

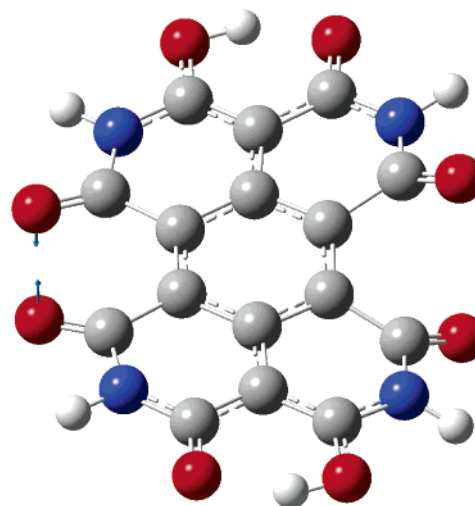


FIGURE 9. The normal mode of the transition state between the meso form and enantiomer a obtained from B3LYP/6-31G(d) calculations.

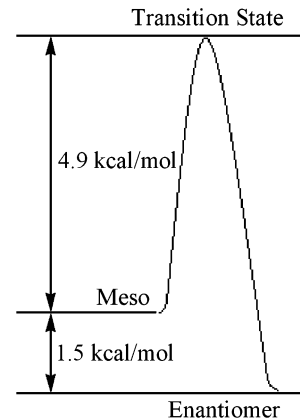


FIGURE 10. Relative DFT energies of the meso form, the enantiomeric form, and the transition state.

estimate of the relative energies in aqueous solution because of the very small conformational change of the carbonyls involved in the interconversion of the three forms (meso, transition state, and enantiomer). It is therefore assumed that the solvation energies are similar for all three forms.

Compound 8 represents a new structural prototype for potential lumazine synthase inhibitors. This is a welcome advancement because although the previously synthesized substrate, intermediate, and product analogue inhibitors of lumazine synthase have proven to be valuable structural and mechanistic probes, their potential antibiotic activity is limited by the presence of a very hydrophilic ribityl side chain.<sup>15,23-31</sup> It is possible that the perylenehexaone system 8 may provide a

new platform for the design of additional lumazine synthase inhibitors with promising biological activities.

## Experimental Section

**1,3,6,8-Tetrahydroxy-2,7-naphthyridine (7).**<sup>7</sup> Malononitrile (**5**) (100 mg, 1.52 mmol) and diethyl acetonedicarboxylate (**6**) (272 mg, 1.35 mmol) were added to anhydrous ethanol (5 mL). One drop of diethylamine was added to the solution. The reaction mixture was stirred for 48 h. The solvent was removed to provide a residue. Sulfuric acid (70%, 0.2 mL) was added to the residue, and the mixture was heated at 100 °C for 10 min. The mixture was cooled to room temperature and then poured into water (0.6 mL). The aqueous solution was filtered to provide a yellow solid product (236 mg, 90%): mp >350 °C (dec). The NMR spectra are consistent with a mixture of lactam and lactim tautomers: <sup>1</sup>H NMR (300 MHz DMSO-*d*<sub>6</sub>) δ 11.37 (s, relative intensity 1.00, exchangeable with D<sub>2</sub>O), 5.76 (s, relative intensity 1.01, exchangeable with D<sub>2</sub>O), 5.50 (s, relative intensity 0.34, exchangeable with D<sub>2</sub>O); <sup>13</sup>C NMR (300 MHz DMSO-*d*<sub>6</sub>) δ 169.5, 169.28, 165.8, 163.6, 162.5, 150.0, 148.7, 104.7, 89.1, 35.67; ESI HRMS calcd for C<sub>8</sub>H<sub>7</sub>N<sub>2</sub>O<sub>4</sub> (MH<sup>+</sup>) 195.0406, found 195.0403. Anal. Calcd for C<sub>8</sub>H<sub>6</sub>N<sub>2</sub>O<sub>4</sub>: C, 49.49; H, 3.12; N, 14.43. Found: C, 49.14; H, 3.08; N, 14.05.

**4,10-Dihydroxy-5,11-dihydro-2,5,8,11-tetraazaperylene-1,3,6,7,9,12-hexaone (8).** Compound **7** (200 mg) was dissolved in hot DMSO (50 mL) to make a saturated solution. The solution was stored at room-temperature open to air. A week later the solution had changed from light yellow to dark red. After a month a dark red crystalline solid (20 mg, 10%) formed in the solution: mp 390 °C (dec). <sup>13</sup>C NMR (DMSO-*d*<sub>6</sub>) δ 170.5, 170.4, 165.5, 162.6, 160.4, 134.1, 124.2, 82.9; ESI HRMS calcd for C<sub>16</sub>H<sub>7</sub>N<sub>4</sub>O<sub>8</sub> (MH<sup>+</sup>) 383.0264, found 383.0264. The crystal structure was solved by X-ray diffraction analysis and the data are summarized as follows: C<sub>24</sub>H<sub>30</sub>N<sub>4</sub>O<sub>12</sub>S<sub>4</sub>; FW = 694.78; *a* = 5.5393(5) Å; *b* = 11.6122(12) Å; *c* = 11.7393(11) Å; α = 76.437(6)°; β = 86.662(6)°; γ = 88.973(6)°; vol = 732.80(12) Å<sup>3</sup>; triclinic; space group *P*-1 (No. 2); *Z* = 1; crystal size = 0.44 × 0.13 × 0.10 mm; GOF = 0.955; *R*(*F*<sub>o</sub>) = 0.047; *R*<sub>w</sub>(*F*<sub>o</sub><sup>2</sup>) = 0.110. Anal. Calcd for C<sub>8</sub>H<sub>6</sub>N<sub>2</sub>O<sub>4</sub>·2DMSO: C, 44.61; H, 3.37; N, 10.40. Found: C, 44.20; H, 3.34; N, 10.46.

***S. pombe* Lumazine Synthase Assay.** Assay mixtures contained 50 mM Tris hydrochloride, pH 7.0, 100 mM NaCl, 5 mM EDTA, 1% (v/v) DMSO, 5 mM dithiothreitol, 100 μM **2**, 1.65 μg of lumazine synthase (specific activity, 16 μmol mg<sup>-1</sup> h<sup>-1</sup>) and variable concentrations of **1** (3 – 20 μM) in a volume of 1 mL. Assay mixtures were prepared as follows. A solution (950 μL) containing 103 mM NaCl, 5.1 mM EDTA, 5.1 mM dithiothreitol, 105 μM **2**,

1.73 μg of lumazine synthase in 51 mM Tris hydrochloride, pH 7.0, was added to 25 μL of inhibitor in 40% (v/v) DMSO (inhibitor concentration window, 0–400 μM) in a cuvette of a six-cell spectrophotometer. The mixtures were incubated at 37 °C, and the reaction was started by adding 25 μL of a solution containing 103 mM NaCl, 5.1 mM dithiothreitol, and substrate **1** (120 – 800 μM) in 51 mM Tris hydrochloride, pH 7.0. The formation of 6,7-dimethyl-8-ribityllumazine (**3**) was measured online for the period of 15 min with a computer-controlled photometer at 408 nm (ε<sub>lumazine</sub> = 10200 M<sup>-1</sup> cm<sup>-1</sup>). The velocity–substrate data were fitted for all inhibitor concentrations with a nonlinear regression method using the program DynaFit.<sup>20</sup> Different inhibition models were considered for the calculation. *K*<sub>i</sub> and *K*<sub>is</sub> values ± standard deviations were obtained from the fit under consideration of the most likely inhibition model as described earlier.<sup>32</sup> For kinetic assays in phosphate buffer, Tris hydrochloride and NaCl in the reaction mixtures were replaced by 100 mM K/Na-phosphate pH 7.0. All other assay parameters in phosphate buffer were the same as described above.

**Molecular Modeling Procedure for the Meso Conformer of 8 (Figure 6).** The X-ray crystal structure of *S. pombe* lumazine synthase (1KYV)<sup>15</sup> in complex with riboflavin was downloaded from the PDB. The C- and N-terminal groups were fixed to be charged using Sybyl (Tripos, Inc., version 7.1, 2005). Hydrogens were added to the protein and to the oxygens of the water molecules. The MMFF94s force field was employed to minimize the energies of the hydrogens to a termination gradient of 0.05 kcal/mol. During this minimization, the heavy atoms of the protein structure and the oxygens of the water molecules were held in a rigid aggregate. Then the energy of the whole complex was minimized using the same method as above. The riboflavin and the phosphate in the binding cavity were removed from the minimized enzyme complex to obtain an apoenzyme structure. By using Gold (BST, version 3.0, 2005), compound **8** was docked into the enzyme to provide a complex that was minimized in two steps. First, the hydrogens and the ligand in the binding cavity were minimized by the conjugate gradient method to a termination gradient of 0.05 kcal/mol while the MMFF94s force field was employed. During this minimization the heavy atoms of the protein structure and oxygens of water molecules were aggregated. Second, the energy of the whole complex was minimized using the same method as described above.

**Acknowledgment.** This research was made possible by NIH grants GM51469 and R21 NS053634, as well as by support from the Fonds der Chemischen Industrie and the Hans Fischer Gesellschaft. The KU-High Throughput Screening Laboratory was established through funding from the National Institutes of Health COBRE award 1 P20 RR15563, from the State of Kansas, and the University of Kansas. We thank the Rosen Center for Advanced Computing (RCAC), Purdue University, for providing the computing facilities used for the ab initio quantum mechanics calculations.

**Supporting Information Available:** CIF file for the crystal structure of compound **8**, the three structures used to produce Figure 7, and tables of total energies and atom coordinates to document calculations. This material is available free of charge via the Internet at <http://pubs.acs.org>.

JO062246D

(23) Cushman, M.; Patrick, D. A.; Bacher, A.; Scheuring, J. *J. Org. Chem.* **1991**, *56*, 4603–4608.

(24) Cushman, M.; Patel, H. H.; Scheuring, J.; Bacher, A. *J. Org. Chem.* **1992**, *57*, 5630–5643.

(25) Cushman, M.; Patel, H. H.; Scheuring, J.; Bacher, A. *J. Org. Chem.* **1993**, *58*, 4033–4042.

(26) Goetz, J. M.; Poliks, B.; Studelska, D. R.; Fischer, M.; Kugelbrey, K.; Bacher, A.; Cushman, M.; Schaefer, J. *J. Am. Chem. Soc.* **1999**, *121*, 7500–7508.

(27) Gerhardt, S.; Schott, A.-K.; Kairies, N.; Cushman, M.; Illarionov, B.; Eisenreich, W.; Bacher, A.; Huber, R.; Steinbacher, S.; Fischer, M. *Structure* **2002**, *10*, 1371–1381.

(28) Zhang, X.; Meining, W.; Cushman, M.; Haase, I.; Fischer, M.; Bacher, A.; Ladenstein, R. *J. Mol. Biol.* **2003**, *328*, 167–182.

(29) Koch, M.; Breithaupt, C.; Gerhardt, S.; Haase, I.; Weber, S.; Cushman, M.; Huber, R.; Bacher, A.; Fischer, M. *Eur. J. Biochem.* **2004**, *271*, 3208–3214.

(30) Morgunova, K.; Meining, W.; Illarionov, B.; Haase, I.; Jin, G.; Bacher, A.; Cushman, M.; Fischer, M.; Ladenstein, R. *Biochemistry* **2005**, *44*, 2746–2758.

(31) Ramsperger, A.; Augustin, M.; Schott, A. K.; Gerhardt, S.; Krojer, T.; Eisenreich, W.; Illarionov, B.; Cushman, M.; Bacher, A.; Huber, R.; Fischer, M. *J. Biol. Chem.* **2006**, *281*, 1224–1232.

(32) Cushman, M.; Jin, G.; Illarionov, B.; Fischer, M.; Ladenstein, R.; Bacher, A. *J. Org. Chem.* **2005**, *70*, 8162–8170.